



HAL
open science

Human macrophages and osteoclasts resorb β -tricalcium phosphate in vitro but not mouse macrophages

Baptiste Arbez, Florence Manero, Guillaume Mabileau, H el ene Marchand-Libouban, Daniel Chappard

► To cite this version:

Baptiste Arbez, Florence Manero, Guillaume Mabileau, H el ene Marchand-Libouban, Daniel Chappard. Human macrophages and osteoclasts resorb β -tricalcium phosphate in vitro but not mouse macrophages. *Micron* (Oxford, England: 1993), 2019, 125, pp.102730. 10.1016/j.micron.2019.102730 . hal-02869318

HAL Id: hal-02869318

<https://univ-angers.hal.science/hal-02869318>

Submitted on 20 Jul 2022

HAL is a multi-disciplinary open access archive for the deposit and dissemination of scientific research documents, whether they are published or not. The documents may come from teaching and research institutions in France or abroad, or from public or private research centers.

L'archive ouverte pluridisciplinaire **HAL**, est destin ee au d ep ot et  a la diffusion de documents scientifiques de niveau recherche, publi es ou non,  emanant des  tablissements d'enseignement et de recherche fran ais ou  trangers, des laboratoires publics ou priv es.



Distributed under a Creative Commons Attribution - NonCommercial 4.0 International License

MANUSCRIPT # JMIC_2019_75 revised version

Human macrophages and osteoclasts resorb β -tricalcium phosphate *in vitro* but not mouse macrophages

Baptiste ARBEZ ^a, Florence MANERO ^b, Guillaume MABILLEAU ^a,
Hélène LIBOUBAN ^a, Daniel CHAPPARD ^{a,b}

^a *Groupe Etudes Remodelage Osseux et bioMatériaux, GEROM, EA 4658, LabCom NextBone, SFR 4208, UNIV Angers, IRIS-IBS Institut de Biologie en Santé, CHU d'Angers, 49933 ANGERS Cedex -FRANCE.*

^b *Service Commun d'Imagerie et Analyses Microscopiques, SCIAM, UNIV Angers, IRIS-IBS Institut de Biologie en Santé, CHU d'Angers, 49933 ANGERS Cedex -FRANCE.*

Please send all correspondence to:

* Daniel CHAPPARD, M.D., Ph.D.

Tel: (33) 244 68 83 43

GEROM

IRIS-IBS Institut de Biologie en Santé,
Université d'Angers

e-mail: daniel.chappard@univ-angers.fr

CHU d'Angers,
49933 ANGERS Cedex -FRANCE

Short running title: Macrophages and osteoclasts resorb β -TCP.

Abstract:

β -TCP is a resorbable bony biomaterial but its biodegradation mechanisms *in vivo* remains unclear. Osteoclast can resorb β -TCP but a role for macrophages has also been suggested by *in vivo* studies. However no *in vitro* study has clearly evidenced the action of macrophages in the resorption process. We prepared flat β -TCP tablets with a smooth surface to investigate the *in vitro* capability of murine (RAW 264.7) and human macrophage cells (PBMCs) to resorb the biomaterial. In parallel, these cells were differentiated into multinucleated osteoclasts with M-CSF and RANK-L. The action of these cells was evaluated by scanning electron microscopy and Raman microspectroscopy after a 21 day culture on the tablets. Human macrophages and osteoclasts derived from PBMCs appeared able to resorb β -TCP by forming resorption pits at the surface of the flat tablets. RAW macrophages were unable to resorb β -TCP but they exhibited this possibility when they have been differentiated into osteoclasts. These cells can engulf β -TCP grains in their cytoplasm as evidenced by light and TEM microscopy with production of carbonic anhydrase (revealed by the immunogold technique in TEM). The resorbed areas were characterized by severe degradation of the grains showing speckled and stick-like aspects indicating a chemical corrosion. The effect was maximal at the grain boundaries which have a slightly different chemical composition. Changes in the Raman spectrum were observed between the resorbed and un-resorbed β -TCP suggesting crystal modifications. In contrast, un-differentiated murine macrophages were not able to chemically attack β -TCP and no resorption pit was observed. RAW cell is not a representative model of the macrophage-biomaterial interactions that occur in human. This *in vitro* study evidences that both human osteoclasts and macrophages represent active cell populations capable to resorb β -TCP.

Keywords:

Beta tricalcium phosphate; macrophage; osteoclast; biomaterial; carbonic anhydrase; Raman.

1. INTRODUCTION

Beta-tricalcium phosphate (β -TCP) is a synthetic biocompatible ceramic that belongs to the calcium orthophosphate family (Dorozhkin, 2017). Its chemical composition (β - $\text{Ca}_3(\text{PO}_4)_2$), close to the mineral phase of bone, allows its use as a bone substitute for filling bone defects in neurosurgery, odontology, maxillo-facial and orthopaedic surgery. β -TCP is recognized as osteoconductive as it provides a resorbable template for the formation of new bone (Bohner et al., 2012; Guillaume, 2017; Hernigou et al., 2017; Tanaka et al., 2017).

Degradation of calcium phosphate (Ca-P) ceramics implies an active cell process (resorption) by cells of the macrophage lineage (Detsch et al., 2008). Although β -TCP is known to be more easily resorbable than hydroxyapatite (the mineral phase of the bone matrix), the mechanism of its resorption remains unclear at the cell level. *In vivo* studies have shown that both mononuclear macrophages and multinucleated osteoclasts are implied in the biomaterial breakdown (Chappard et al., 2010; Pascaretti-Grizon et al., 2017; Suba et al., 2006; Zerbo et al., 2005). Analysis of human bone biopsies have shown that osteoclasts can be identified by a histoenzymatic technique identifying tartrate resistant acid phosphatase (TRAcP), an intracytosolic enzyme responsible for intracellular breakdown of the organic phase of the bone matrix (Chappard et al., 2010; Halleen et al., 1999; Tanaka et al., 2017). In parallel, the presence of a population of macrophages whose cytoplasm is filled with β -TCP elementary grains is also observed on histological sections and nanocomputed tomographic images (Pascaretti-Grizon et al., 2017). So, a double population seems to be responsible for the resorption of β -TCP. We have previously shown, in an *in vitro* study by time-lapse microscopy that β -TCP granules can be attacked by macrophages (Beuvelot et al., 2011). However, no scanning electron microscopic (SEM) studies on the biomaterial have unequivocally evidenced resorption lacunae caused by macrophages (Beuvelot et al., 2011; Detsch et al., 2010; Schaefer et al., 2011).

The aims of this study were to investigate the *in vitro* resorption of β -TCP by human peripheral blood mononuclear cells (PBMCs) and murine macrophages (RAW 264.7) by scanning electron microscopy (SEM). The cytokines M-CSF (macrophage colony stimulating factor) and RANKL (ligand for the receptor-activator of nuclear factor κ B) were also added on both types of cells to induce the differentiation into osteoclasts on plane β -TCP tablets. Immunogold analysis of RAW 264.7 macrophages was done by TEM to identify carbonic anhydrase, a key enzyme implied in the degradation of the mineralized phase of calcified tissues (Laitala and Väänänen, 1993).

2. MATERIAL AND METHODS

2.1 Preparation of β -TCP tablets with a plane surface

A β -TCP slurry was obtained from Kasios (L'Union, France). It was composed of a powder of elementary β -TCP grains mixed with a binder and a dispersing agent. The β -TCP slurry was poured into hydrophobic plastic Petri's dishes containing polypropylene rings, 1.5 cm in diameter. The slurry was poured into each ring (0.5 mL) and was subsequently dried for 24 hours at room temperature. This produced dried tablets that were removed and sintered at high temperature (1200°C) in a laboratory furnace (Model MRF1, Vecstar Furnaces, Chesterfield, UK) to obtain the final β -TCP tablets with a perfectly plane surface. These tablets were used in 24-well plates for cell culture. Surface roughness of the β -TCP tablets was analyzed using a Wyko NT 9100 vertical scanning interference microscopy (Bruker Nano Surface, Palaiseau, France). We previously analyzed the β -TCP biomaterial by XRF (dispersive X-ray fluorescence spectrometry) in a previous paper and confirmed its purity (Pascaretti-Grizon et al., 2017). Prior to cell seeding, β -TCP tablets were sterilized in 70% ethanol during 24 hours and dried for an hour at room temperature.

2.2 Characterization of the biomaterial by Raman spectroscopy

The chemical spectrum of the β -TCP tablets was analyzed by Raman spectroscopy on a Renishaw InVia Qontor microscope (equipped with a Leica DM2700 microscope, objective 20X, NA 0.40, WD 0.39) with the WiRE 5.0 software (Renishaw, Champs sur

Marne, France). The excitation laser wavelength was 532 nm with an excitation power of 50 mW and a grating of 1800 line/mm resolution. The final spectrum was obtained by averaging five scans of 1 sec each. A concave rubberband base line correction was applied with an x^{11} polynomial equation. Spectra were obtained at the surface of control β -TCP tablets and in areas modified by cell activity on cultured tablets.

2.3 Cell culture reagents and conditions

Alpha-Minimum Essential Medium Eagle (α -MEM), Dulbecco's Modified Eagle Medium (DMEM), heat-inactivated fetal calf serum (FCS), penicillin and streptomycin were purchased from Gibco (ThermoFisher Scientific, Illkirch, France). Macrophage colony-stimulating factor (M-CSF) and soluble human receptor activator of nuclear factor kappa B ligand (shRANK-L; ref: 390-TN) and soluble murine RANK-L (smRANK-L; ref: 462-TEC) were purchased from R&D Systems (Bio-Techne, Lille, France). Histopaque 1077 was purchased from Sigma-Aldrich (Saint-Quentin Fallavier, France). Embed 812® and glutaraldehyde were obtained from Electron Microscopy Sciences (Hatfield, USA).

The β -TCP tablets were immersed overnight in 24-well plates filled with α -MEM supplemented with 100 IU/ml penicillin, 100 μ g/ml streptomycin and 10% FCS (fetal calf serum) to remove any trace of ethanol. This also allowed proteins to adhere onto the β -TCP surface. Macrophage cells were then seeded as described below.

2.4 Human PBMCs cell cultures

2.4.1 Isolation of human PBMCs

Human PBMCs were isolated from 5 buffy coats from venepunctures (Établissement Français du Sang, Angers, France). Blood was diluted (1:1 volume ratio) in α -MEM with 100 IU/ml penicillin and 100 μ g/ml streptomycin and without FCS. Diluted blood was subsequently gently layered over Histopaque 1077 and centrifuged at 330 g for 20 min. PBMCs were retrieved at the Histopaque interface and mixed with α -MEM with penicillin and streptomycin (without FCS). Cells were then washed twice (10 min each) and the supernatants were discarded and replaced by α -MEM with penicillin, streptomycin and 10% FCS at the end of the second centrifugation. Purity of the PBMC preparation

was determined after May-Grünwald-Giemsa staining and was found more than 95% as previously reported by others (Jacob and Sudhakaran, 2001; Lyu and Park, 2005).

2.4.2 Culture of human PBMCs

PBMCs were seeded on the β -TCP tablets at a concentration of $2 \cdot 10^6$ cells per well. Controls were obtained by seeding cells directly on the plastic well. Cells were allowed to adhere for 3 hours; the medium containing all non-adherent cells was then discarded and replaced by fresh medium supplemented with M-CSF 25 ng/mL to ensure the viability and the differentiation to naïve macrophages of PBMCs. In half of the wells, RANK-L (50 ng/mL) was added to the medium 7 days after seeding to induce differentiation into osteoclasts. This procedure was used to compare the activity between PBMCs and osteoclastic cells generated with the cytokine cocktail (M-CSF + RANK-L). In both conditions, cells were cultured during 21 days and were maintained in a humidified atmosphere of 5% CO₂ at 37°C; the culture medium was replaced every 2 or 3 days.

2.5 Mouse monocytes/macrophages cell cultures

The mouse monocyte/macrophage cell line Raw264.7 (American Type Culture Collection ATCC #TIB-71, Molsheim, France) was used. Cells were seeded on the β -TCP tablets in 24-well plates (21 250 cells per well) in α -MEM medium supplemented with 25 ng/mL M-CSF. Cells were cultured for 21 days without RANK-L and with RANK-L, 50 ng/mL, to induce osteoclast differentiation. They were either fixed or lysed for SEM analysis as described above.

2.6 SEM analysis

Analyses were done on a JEOL 6301F (JEOL, Paris, France). All samples were coated with a 20 nm layer of platinum by sputtering with a high vacuum coater (Leica EM ECA600, Leica, France). Images were captured in the secondary electron mode with an acceleration tension of 3 kV.

The β -TCP tablets covered by the resorbing cells were washed 3 times in cacodylate buffer (0.2 M, pH 7.4) and fixed overnight at 4°C with glutaraldehyde (2.5% in cacodylate buffer). Half of the tablets were subsequently post fixed with osmium

tetroxide (1% in distilled water for 1 hour). They were dehydrated with a gradient of ethanol, desiccated with hexamethyldisilazane and examined by SEM to analyze the morphology of the cells anchored at the surface of the biomaterial.

Remaining tablets covered by cells were treated overnight with ammonia hydroxide 1M to gently lyse the cells, then washed in MilliQ water, sonicated 3 times then placed in absolute ethanol followed by complete evaporation at room temperature in a similar way as one of our previous studies (Mabilleau et al., 2012). This produced de-cellularized tablets on which resorption areas can be identified as pits at the surface. Control β -TCP tablets were similarly treated in ammonia hydroxide 1M to see if this protocol altered the biomaterial surface.

For each de-cellularized β -TCP sample, ten SEM images were taken at a working distance of 15 mm and at the same magnification and transferred in ImageJ (ImageJ 1.52, NIH). The SEM images were binarized and thresholded: the un-resorbed material appeared in white and resorption lacunae in black. Resorption surface area was defined as the ratio of black pixels over white pixels. The average area of the resorption pits was determined on the same binarized SEM images. The outlines of the resorption pits were obtained and used with the particle analysis facility of the software. For each pit, the size in μm^2 was calculated and results were expressed as the average size for each sample.

2.7 3D profiles

The InVia Qontor Raman microscope (Renishaw, Champs sur Marne, France) was used with the WiRE 5.0 software to acquire 3D profiles on the de-cellularized β -TCP tablets. A 532 nm laser was used for 0.5 s at 2.5 mW for each point of the map with a 0.5 μm distance between each point. The Live Track TM technology was used to automatically maintain the focus during data collection. The depth of resorption pits was measured on ten pits for each culture condition. The x - y images were obtained with a minimum of 400 * 400 μm , the z dimension was determined by focusing the laser at the surface of the β -TCP pellet. 3D maps were obtained and the tilt correction was done with the SurfCharJ.

plugin for ImageJ (Chinga et al., 2007). The depth of the resorption pit was determined as the maximum z for each resorption pit.

2.8 Cytological analysis

PBMCs were cultured during 21 days in contact with small fragments prepared from the tablets. They were fixed overnight at 4°C with 2.5% glutaraldehyde as above then washed 3 times in cacodylate buffer at 4°C. They were subsequently washed in MilliQ water and dehydrated in increasing ethanol concentrations (from 50% to 100%). Samples were transferred in a glass tube containing propylene oxide for 30 min at room temperature then in propylene oxide/Embed812 (50/50) overnight and finally in the pure epoxy resin (Embed 812®) for 4 h which was polymerized at 60°C for 48 h. Blocks were cut on a Leica UC-7 ultramicrotome (Leica Microsystems, Heidelberg, Germany) equipped with a diamond knife. Sections (2 µm in thickness) were stained with azure blue II/methylene blue and observed by light microscopy.

2.9 Transmission electron microscopy

Immunolabeling of carbonic anhydrase was performed on control Raw264.7 and PBMCs cultured on plastic in α -MEM medium supplemented with 25 ng/mL M-CSF for 7 days. Additional cells were similarly cultured on β -TCP granules with M-CSF or M-CSF + RANK-L (25 ng/mL) as above. They were rinsed in phosphate buffer (0.1 M pH 7.4) and fixed in glutaraldehyde (2.5% in phosphate buffer) for ultrastructural analysis or in paraformaldehyde (2.5%) and glutaraldehyde (0.5%) in phosphate buffer for immunolabeling.

For morphological analysis, cells were then rinsed in the phosphate buffer and post fixed for one hour in osmium tetroxide (1% in distilled water). They were dehydrated in a graded alcohol series, then transferred in propylene oxide before embedding in Epon.

For immunolabeling, cells were then rinsed in distilled water, dehydrated as above and embedded at -20°C in Lowicryl (Lowicryl Monostep K4M polar, EMS, Hatfield, USA). Blocks were sectioned on a Leica UC-7 ultra-microtome (Leica Microsystems, Heidelberg, Germany) and transferred on copper or nickel grids.

For immunolabeling, the grids were placed on a drop of glycine (0.2M in distilled water) then rinsed in the phosphate buffer. They were then incubated during 30 min. in the blocking solution (Blocking Solution for goat gold conjugates, ref. 905.002, Aurion, Wageningen, Netherlands) and extensively rinsed in the phosphate buffer. Grids were then incubated with the primary antibody against type II carbonic anhydrase (Anti-Carbonic Anhydrase II, antibody ab191343, Abcam, Cambridge, UK) with a 1/40 dilution during one hour at room temperature. After rinsing, the secondary antibody coupled with gold nano-beads (Sigma-Aldrich, Saint-Louis, USA - dilution 1/100) was applied during one hour at room temperature. They were then rinsed in distilled water followed by incubation for 10 min. in glutaraldehyde (2% in the phosphate buffer) and a final rinse in water.

Grids for morphological analysis or immunolabeling were contrasted with 3% uranyl acetate in 50° alcohol, rinsed in distilled water and let dried on Whatman® paper. Analysis was done with a Jeol JEM-1400 transmission electron microscope (Jeol, Paris, France), with an acceleration voltage of 120 kV.

2.10 Statistical analysis

Statistical analysis was performed with Systat statistical software (Systat, San José, CA, release 13.00.05). All data are expressed as mean \pm SEM. Differences between the different culture conditions were analyzed by a Kruskal-Wallis non parametric ANOVA followed by a Mann-Whitney U test for pair-wise comparisons. A difference was considered as significant when $p < 0.05$.

3. RESULTS

3.1 β -TCP tablets characterization

The tablets prepared by our method were flat with a smooth surface; the arithmetic average roughness (Ra) of the tablets, as determined by vertical scanning interference microscopy, ranged from 300 to 350 nm.

3.1.1 Raman spectroscopy

The Raman spectrum of β -TCP tablets showed internal vibrations characteristic of the PO_4^{3-} tetrahedral groups of the β -TCP crystal as described in the literature (Kumar et al., 2015; Pascaretti-Grizon et al., 2011). The symmetric stretching (ν_1) of P-O bonds of the tetrahedron corresponded to the peaks with the highest intensity at around 948 cm^{-1} and 970 cm^{-1} . The asymmetric stretching (ν_3) had a lower intensity and was located in the $1017\text{-}1090\text{ cm}^{-1}$ range. The other vibrational modes (ν_2 and ν_4) correspond to O-P-O bending deformations of the tetrahedron. They were respectively located at 406 and 547 cm^{-1} .

3.1.2 SEM

The β -TCP elementary grains coming from the colloidal suspension in the slurry were clearly visible before sintering (Fig. 1A). After sintering, the tablet surfaces appeared flat at low magnification (Fig. 1C) with a polygonal pavement (Fig. 1B). Polygonal tiles were separated from each other by grain boundaries. The overnight treatment with NH_4OH (used for de-cellularization) did not alter the surface of the sintered pellets (Fig. 1D).

3.2 *Culture with macrophage cells*

3.2.1 Mouse macrophages

RAW cells cultured had most frequently a round shape with a diameter ranging from 10 to $20\text{ }\mu\text{m}$ (Fig. 2A). Cells emitted numerous filopodia that directly anchored them to the surface of β -TCP. Cytoplasmic veil-like structures were observed at the apical cell surface (Fig. 2B). Tilted images from the de-cellularized samples failed to evidence any resorption lacuna (Fig. 2C).

3.2.2 Human macrophages

PBMCs appeared round and stretched with size ranging from $10\text{ }\mu\text{m}$ in diameter and up to $100\text{ }\mu\text{m}$ in length (Fig. 3A-B-C). Round shaped and stretched cells were directly anchored to the β -TCP by filopodia. De-cellularized samples clearly evidenced resorption lacunae on the β -TCP surfaces (Fig. 3D). The eroded lacunae ranged from 100 to $200\text{ }\mu\text{m}$ in diameter. The lacunae were characterized by noticeable changes occurring at the biomaterial surface (Fig. 3E). The top half part of fig. 3E shows a non-resorbed area while

the bottom part shows the edge of a resorption pit. In these areas, grains situated at the edges of lacunae were partly detached giving a chaotic aspect of the erosion pit. Grains at the bottom of the lacunae were severely corroded and showed stick-like surface alterations at higher magnifications, suggesting a chemical corrosion (Fig. 3F). Grain boundaries seemed preferably attacked as deep grooves were observed that tend to separate the previously sintered grains (Fig. 3F).

Cytological staining of semi thin sections evidenced that human macrophages derived from PBMCs were able to phagocyte elementary grains of β -TCP (Fig. 4). Some elementary grains of β -TCP were entirely absorbed in the cytoplasm of cells.

3.3 Culture with cells differentiated into osteoclasts

3.3.1 Mouse osteoclasts

SEM images showed the presence of flat giant cells with diameter ranging from 100 to 400 μm (Fig. 5A). Signs of surface alteration of the β -TCP tablets were found in the immediate vicinity of the cells as described above (Fig. 5B). Some grains evidenced surface corrosion with stick-like alterations at high magnifications. Grain boundaries were severely eroded giving the aspect of a dislocated surface (Fig. 5C).

The de-cellularized samples clearly showed resorption pits (Fig. 5D-E). Samples showed numerous resorption lacunae randomly disposed at the surface of the β -TCP tablets. They ranged from 100 to 300 μm in diameter leading to an increased surface roughness with dislocated grains in the eroded areas. The grains at the bottom of the lacunae evidenced net signs of corrosion at higher SEM magnifications. Grain boundaries were preferably attacked and deep grooves tend to separate them (Fig. 5F).

3.3.2 Human osteoclasts

Giant flat cells were observed (around 80 μm in diameter) covering the surface of the biomaterial, they were associated with round or elongated mono-nucleated cells (Fig. 6A). Signs of resorption of the β -TCP biomaterial were observed in the vicinity of the giant cells with dislocation of the sintered grains and a hedgehog aspect of some grain surfaces (Fig. 6B-C).

On the de-cellularized tablets, the presence of numerous resorption lacunae was evidenced as holes with irregular boundaries (Fig. 6D-E). When compared to the control, the samples clearly evidenced resorption lacunae (Fig. 6E). The lacuna areas ranged from 50 to 200 μm in diameter and their boundaries presented numerous dislocated grains (Fig. 6F). The surface of the grains inside the resorption area presented numerous spikes indicating a severe corrosion of the crystals.

3.4 Transmission electron microscopy

The RAW cells or the PBMCs cultured on plastic without growth factor had a round (Fig. 7A) shape and were multinucleated in the presence of RANKL (data not shown). When cultured on the β -TCP granules, they appeared to internalize in their cytoplasm large crystals of the biomaterial (Fig. 7A). The biomaterial was fragile and brittle during microtomy. Under the electron beam, it appears as black particles inside vacuoles (Fig. 7B-C).

Carbonic anhydrase labeling was characterized by the presence of gold nanobeads diffusely scattered in the cytoplasm or aggregated into small clusters in undifferentiated cells (Fig. 7D-E). In osteoclast prepared from cells were cultured with M-CSF + RANKL, the number of gold nanobeads was markedly increased in the cytoplasm and they tend to form larger clusters (Fig. 7F).

3.5 Raman analysis of β -TCP in the eroded areas

Raman spectra were taken on a control β -TCP tablet (Fig. 8A) and at the bottom of resorption pits made on β -TCP by differentiated and un-differentiated PBMCs. The spectrum of a β -TCP tablet immersed 21 days in the culture medium did not differ from the control sample (data not shown). On the control tablet spectrum, the 948 peak had a lower intensity than the 970 peak.

In contrast, inside the resorption pits due to PBMCs, the intensity of the 970 peak was markedly reduced and becomes convoluted with the 948 peak (Fig. 8B). Positions of the other peaks and their relative intensities remained unchanged. The 948 and 970 peaks correspond to P-O bonds of the PO_4^{3-} tetrahedron. The cellular degradation led to a modification of these bonds.

Figure 9 shows the 3D profiles of β -TCP tablets after culture and de-cellularization. The control tablets presented a smooth surface (Fig. 9A). No pits were observed on tablets cultured with un-differentiated RAW cells (Fig. 9B). Tablets seeded with osteoclasts differentiated from RAW cells had shallow erosion zones scattered on the surface (Fig. 9C). They combined together to form extended shallow eroded areas. Each resorption lacuna made by un-differentiated human cells was composed of a single deep pit at the surface of the biomaterial (Fig. 9D). Differentiated human cells eroded the biomaterial deeper than the un-differentiated human cells (Fig. 9E).

3.6 Quantitative analysis

Figure 10 shows the average depth, the percentage of eroded areas, the average pit size and the images used for computation. No significant difference was observed between differentiated and un-differentiated human cells for eroded areas and size of resorption pit; the resorption pits were somewhat deeper with differentiated macrophages although the difference did not reach significance. Un-differentiated mouse cells appeared unable to erode the biomaterial, however after differentiation, they gained the capability to dig resorption pits that were less deep than those created by human cells ($p < 0.025$).

4. DISCUSSION

In the present study, we have prepared very flat β -TCP tablets to analyze the onset of resorption areas when macrophages or osteoclasts (differentiated from mononuclear macrophage precursors) were seeded at the surface.

We found that only osteoclasts differentiated with M-CSF and RANK-L from RAW cells were able to resorb β -TCP tablets and that undifferentiated RAW macrophages did not create resorption pits. However, both macrophages and osteoclasts differentiated from human PBMCs presented the ability to resorb β -TCP. The attacked grains showed spikes on their surface, suggesting a chemical dissolution of β -TCP and deep grooves were evidenced between the sintered grains, indicating a preferential and more potent attack in this location.

Several studies have used the mouse RAW 264.7 model *in vitro* due to the availability of the cells to investigate β -TCP resorption but results are contradictory. Some studies

showed that dense and porous β -TCP is not resorbed by differentiated RAW 264.7 cells after 21 days (Detsch et al., 2010; Schaefer et al., 2011). However, results from other studies are in accordance with our findings, showing that mouse osteoclasts differentiated from RAW cells can resorb β -TCP (Clarke et al., 2017; Roy et al., 2013; Xia et al., 2006a). In the present study, we compared β -TCP resorption due to macrophage and osteoclast cells of murine and human origin and marked differences were observed. Human macrophages were able to resorb and phagocytize *in vitro* β -TCP grains while mouse macrophages appeared unable to do this by SEM, 3D imaging or Raman spectroscopy. Human macrophages and osteoclast differentiated with M-CSF + RANKL from PBMCs attacked the biomaterial surface and dug resorption pits. In a previous study, only osteoclasts differentiated human cells were found to resorb β -TCP (Davison et al., 2014). Quantitative image analysis showed that mouse osteoclasts led to larger but less deep resorption pits than human cells in the present study. Mouse osteoclasts were larger in SEM than human osteoclasts differentiated PBMCs and created larger resorption pits (Lees et al., 2001). Resorption lacunae created by mouse osteoclasts appeared composed of numerous small local erosion pits whereas human cells dug fewer but deeper pits. On tablets cultured with macrophages or osteoclasts, elongated mononucleated cells were observed as classically reported with macrophages in long term culture (Zuckerman et al., 1979). Their implication in the biomaterial resorption together with osteoclast is probable and the morphometric analysis of the resorption pits takes this possibility into account.

The SEM and Raman analysis of the resorption pits found in the present study suggest a chemical dissolution of the crystal. The grain boundaries were more seriously attacked indicating a higher dissolution rate of the grain boundaries than of the crystallites. In polycrystalline materials, grain boundaries are known to be amorphous instabilities where impurities can segregate if their solubility in the crystal is reached. In acidic microenvironments, corrosion is known to preferentially occur at grain boundaries due to the rapid dissolution of the amorphous impurities residing there (Ćurković et al., 2008; Kishi et al., 1997; Mikeska et al., 2000). Raman spectra showed a modification of P-O bonds of the PO_4^{3-} tetrahedron corresponding to a chemical dissolution as well. The Raman spectra modifications observed are similar to those found on β -TCP grains in

cytoplasm of macrophages in patient after sinus-lift surgeries (Pascaretti-Grizon et al., 2017). Osteoclast possess a mechanism responsible for dissolution of the mineral phase of the bone matrix. They can produce and excrete protons in a subcellular compartment (the resorption chamber) under the ruffled border. They possess a type II cytosolic carbonic anhydrase which produce protons by coupling H₂O and CO₂ and the protons are excreted in the resorption chamber by a membrane-bound H⁺-ATPase (Asotra et al., 1994; Laitala and Väänänen, 1993). In the present study, this enzyme was identified by post-embedding immunolabeling. The label was identified as scattered beads in the cytoplasm of undifferentiated cells or aggregated in small clusters as reported by others in monocyte/macrophages (Karhukorpi, 1991; Sundquist et al., 1987). The osteoclasts differentiated from RAW or PBMC cells contained larger clusters indicating an increase enzyme activity in these cells.

Biodegradation of β -TCP still remains unclear. In bone, multinucleated osteoclasts resorb the calcified matrix to ensure the constant remodeling of the skeleton. Therefore, most *in vitro* studies concerning β -TCP biodegradation have focused on resorption by osteoclasts using mouse RAW 264.7 cells (Detsch et al., 2008; Detsch et al., 2010; Roy et al., 2013; Schaefer et al., 2011). However when analyzing bone biopsies from patients or animals grafted with β -TCP, numerous macrophages are encountered in association with true osteoclasts (Chappard et al., 2010; Pascaretti-Grizon et al., 2017; Suba et al., 2006; Zerbo et al., 2005). Moreover, macrophages are able to phagocytose small β -TCP particles *in vivo* (Chappard et al., 2010; Eggli et al., 1987; Nyangoga et al., 2010; Pascaretti-Grizon et al., 2017; Suba et al., 2006). It was suggested that macrophages stimulate bone resorption when phagocytosing particles (Murray and Rushton, 1990). Clearly, osteoclast is not the only cell lineage involved in β -TCP resorption *in vivo* and we have presented a clear evidence of an *in vitro* macrophagic action on β -TCP by SEM in this present work and by video microscopy elsewhere (Beuvelot et al., 2011). Not only the mouse RAW model is not consistent concerning resorption *in vitro* but it is also mostly used with cells differentiated exclusively into osteoclasts leaving the macrophages resorption aside.

Most *in vivo* studies do not evidence that osteoclastic activity is the unique or main biodegradation process for β -TCP in the human body. TRAcP negative giant cells, formed by fusion of macrophages, are observed in the first steps of degradation of

synthetic or natural ceramics before the onset of true TRAcP+ osteoclasts (Barbeck et al., 2017; Baslé et al., 1993; Dersot et al., 1995). Zerbo et al., did not observe giant cells in biopsies 6 months after sinus floor augmentation graft with β -TCP (Zerbo et al., 2005). However, TRAcP positive cells were present around the β -TCP particles but they were present in small number and contained few nuclei. The authors concluded that osteoclasts had only a limited role in the biodegradation of β -TCP. Another histologic study on biopsies performed 6 months after sinus lift surgeries with β -TCP did not support the osteoclastic resorption of the graft but identified β -TCP particles in the cytoplasm of macrophages (Suba et al., 2006). We have repeatedly reported that both TRAcP+ osteoclasts and macrophages containing phagocytized β -TCP grains are found in human and rabbit bone biopsies after β -TCP implantation but we have not identify inflammatory giant cells (Chappard et al., 2010; Nyangoga et al., 2010; Pascaretti-Grizon et al., 2017). In an animal study performed in the rabbit, we reported that ketoprofen, a non-steroidal anti-inflammatory drug has no effect on the healing of a β -TCP graft confirming the absence of inflammation induced by this synthetic biomaterial (Nyangoga et al., 2010). Macrophages filled with elementary grains of β -TCP are found in the marrow spaces between the newly formed bone trabeculae in such a high amount that they can be visualized by X-ray nanocomputed tomography (Pascaretti-Grizon et al., 2017). They appear very numerous giving a ‘milky way’ appearance in marrow spaces due to the radio-opacity of the β -TCP grains in the cytoplasm of macrophages. In a series of biopsies performed a long time after bone surgery in patients implanted with β -TCP, TRAcP+ osteoclasts were evidenced in direct contact with the biomaterial and other giant cells expressing heterogeneous TRAcP levels as well as macrophages were present in the surrounding tissues (Kucera et al., 2014). The multinucleated osteoclasts differentiated from mouse RAW cells and human PBMCs were found TRAcP positive (data not shown).

In vivo studies tend to show that macrophages are involved in β -TCP resorption but *in vitro* studies do not reflect this tendency with mouse RAW model. In the present study and in the few studies *in vitro* using un-differentiated mouse RAW 264.7 macrophages, no resorption was unequivocally evidenced (Clarke et al., 2017). However, with human macrophages, our findings clearly evidenced resorption of β -TCP by PBMC

macrophages. This suggests that *in vitro* macrophage resorption of β -TCP depends on the macrophage origin (i.e. mouse or human): macrophages from human PBMCs cells resorbed β -TCP *in vitro* whereas murine RAW 264.7 macrophages could not attack the biomaterial surface, even both cells exhibited similar cytological aspect in SEM (veil-like processes) (Arbez and Libouban, 2017). The mouse RAW 264.7 model seems not to be a representative model *in vitro* of macrophage resorption of β -TCP in human. It has been reported that β -TCP up-regulates TNF- α , CCL2 (MIP-1), CCL3 (MIP-1 α), CCL4 (MIP-1 β), CCL5 (RANTES) and CXCL2 (MIP2- α) in mouse macrophages *in vitro* (Tai et al., 2016). However, PBMCs similarly exposed *in vitro* to β -TCP showed an increase of TNF- α , IL-1 β , IL-8 (Lange et al., 2009). Differences in the profile of cytokine secretions between human and murine macrophages may explain the differences observed for β -TCP resorption.

5. CONCLUSION

Our results show that β -TCP is resorbed and phagocytized *in vitro* by both human macrophages and osteoclasts obtained from PBMCs. The use of flat β -TCP tablets allowed an unequivocal identification of the resorption pits at the SEM level. Resorption pits formed during biodegradation led to a corrosion of the β -TCP grains which was maximum at the grain boundaries. Mouse macrophages, which are used in comparison with PBMCs to study the erosion of biomaterials, did not alter the β -TCP surface and no resorption pit occurred (Chamberlain et al., 2009; Xia et al., 2006b; Zhang et al., 2012). However, when they were differentiated using RANK-L and M-CSF, the osteoclasts were able to degrade β -TCP. Un-differentiated RAW 264.7 cells did not appear to be a representative model of the macrophage interactions with β -TCP.

Conflict of interest

BA received a PhD scholarship from Kasios SAS via the ANRT (Association Nationale Recherche Technologie) CIFRE program.

Acknowledgments

This work was made possible by grants, from ANR, program LabCom “NextBone”. SEM and cytological analysis were performed at Service Commun d’Imagerie et d’Analyses Microscopiques (SCIAM), Université d’Angers, thanks to R. Mallet. Many thanks for Kasios SAS, 18, chemin de la Violette 31240 L'UNION – France for providing the slurry and the β -TCP granules.

LEGENDS OF FIGURES

Figure 1: SEM images of β -TCP tablets. A) Before sintering and B) after sintering. The elementary grains have a typical polyhedral aspect and are closely packed together. C) The same sample at a lower magnification to highlight the smooth surface of the biomaterial. D) A control sample after immersion in NH_4OH 1M for 14 hours.

Figure 2: SEM analysis of mouse macrophages cultured 21 days with M-CSF and seeded at the surface of a flat β -TCP tablet. A) Most macrophages have a round shape and are anchored at the surface of the biomaterial. B) Higher magnification showing that a macrophage is anchored at the polygonal surface of the β -TCP tablet. No sign of disorganization of the biomaterial surface can be seen. C) Tilted surface of a de-cellularized tablet confirming the absence of resorption pit.

Figure 3: SEM analysis of human PBMCs cultured 21 days with M-CSF and seeded on a β -TCP tablet. A) Macrophages have either a round or elongated shape and are anchored at the surface of the biomaterial. B) Higher magnification C) macrophages with veil-like processes anchored at the surface of β -TCP tablet. D) Surface of a de-cellularized tablet showing numerous resorption pits, compare with Fig. 1C. E) Edge of a resorption pit showing partly detached grains giving a chaotic aspect. F) Grains at the bottom of a resorbed lacuna are severely corroded and show stick-like surface alterations and grain boundaries seem preferably attacked as deep grooves tend to separate the different grains.

Figure 4: Light microscopy of human PBMCs cultured 21 days with M-CSF in contact with β -TCP (epoxy embedding). β -TCP grains appears in grey and cells in blue, some grains are evidenced in the cytoplasm of the PBMCs.

Figure 5: SEM analysis of differentiated murine RAW 264.7 cells cultured 21 days with M-CSF and RANK-L and seeded on a flat β -TCP tablet. A) A large osteoclast is evidenced (arrowheads) together with small round macrophages at the surface of the biomaterial. B) Higher magnification at the periphery of an osteoclast (arrowheads) near an eroded area. C) Part of an osteoclast near a resorption pit with partly detached grains giving a chaotic aspect. D) Tilted surface of a de-cellularized tablet showing numerous resorption pits. E) A resorption pit at a higher magnification clearly showing the difference between the un-attacked and attacked areas of the tablet; compare with Fig. 1C. F) Grains at the bottom of a resorbed lacuna are severely corroded and show stick-like surface alterations; grain boundaries are preferably attacked with deep grooves that separate the different grains.

Figure 6: SEM analysis of differentiated human PBMCs cultured 21 days with M-CSF and RANK-L and seeded on a flat β -TCP tablet. A) Three large osteoclasts are evidenced together with small round macrophages at the surface of the biomaterial. B) Higher magnification at the periphery of a large osteoclast at the surface of β -TCP. C) Part of an osteoclast covering a resorption area with partly corroded grains. D) Tilted surface of a de-cellularized tablet showing numerous resorption pits. E) A resorption pit at a higher magnification clearly showing the difference between the un-attacked and attacked areas of the tablet, un-tilted image; compare with Fig. 1C. F) Grains at the bottom of a resorbed lacuna are severely corroded and show stick-like surface alterations and grain boundaries are preferably attacked with deep grooves that separate the different grains.

Figure 7: TEM analysis. A) A RAW 264.7 cells without cytoplasmic inclusion of β -TCP; B) a human PBMC cultured in presence of β -TCP granules. The cell has engulfed grains of the biomaterial in its cytoplasm; C) higher magnification of a PBMC with a β -TCP inside a cytoplasmic vacuole; D) a RAW 264.7

cultivated for 7 days on β -TCP granules. Few gold nanobeads are scattered in the cytoplasm (arrow); E) a control RAW 264.7 cultured on plastic without β -TCP, few nanobeads are grouped in a small cluster (arrow); F) a RAW 264.7 treated by M-CSF + RANKL cultivated for 7 days on β -TCP. A large cluster of nanobeads is evidenced.

Figure 8: Raman spectra of the β -TCP material. A) Spectrum obtained on a control β -TCP tablet. B) Spectrum obtained at the bottom of a resorption pit created by PBMCs cultured with M-CSF and RANK-L. Note changes in the 948 and 970 cm^{-1} peaks.

Figure 9: 3D images of resorption pits on β -TCP after 21 days of cultures. The samples were all de-cellularized. A) Control (immersed in medium for 21 days then treated with ammonium hydroxide 1M overnight and washed with MilliQ water) B) un-differentiated RAW cells; C) Differentiated RAW cells; D) un-differentiated PBMCs; E) Differentiated PBMCs.

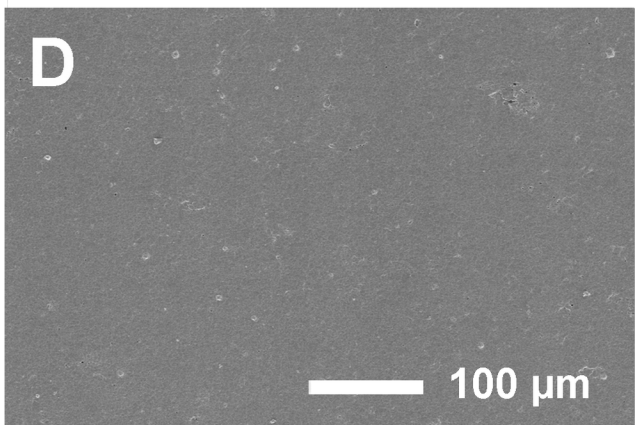
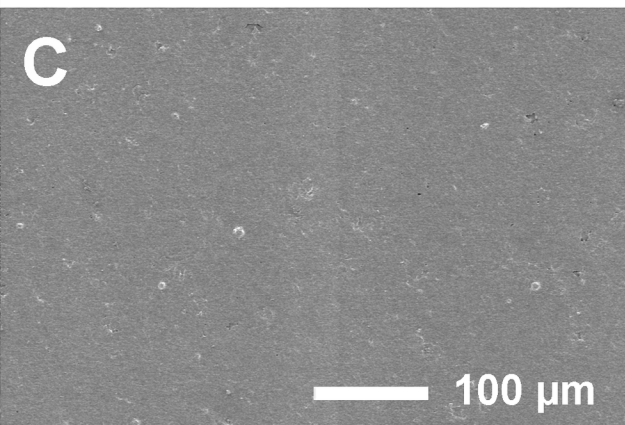
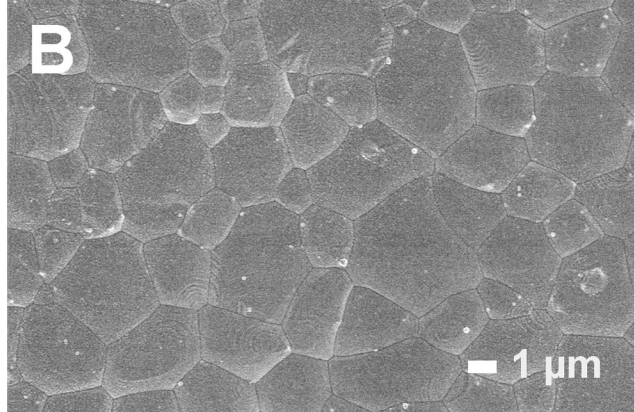
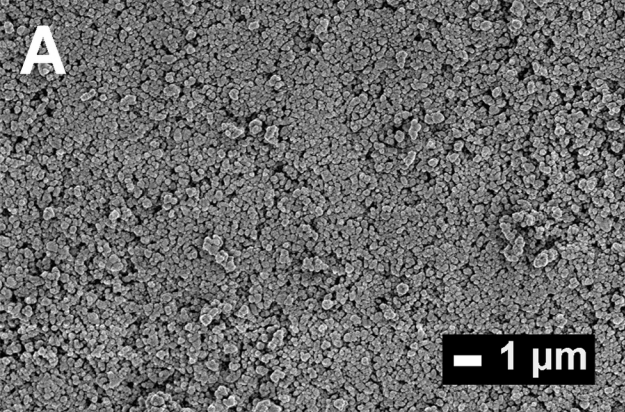
Figure 10: Quantitative analysis of biomaterial erosion by cultured cells. A) Average depth derived from Raman analysis. B) Percent of eroded surface of the flat β -TCP tablets, C) Average size of a resorption pit. D) Principles of computation with ImageJ of parameters on SEM images appearing in B and C.

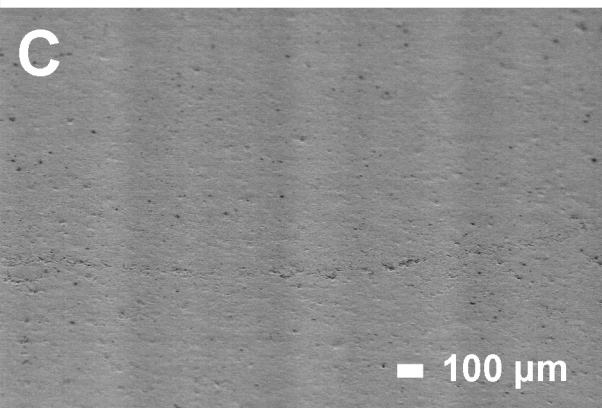
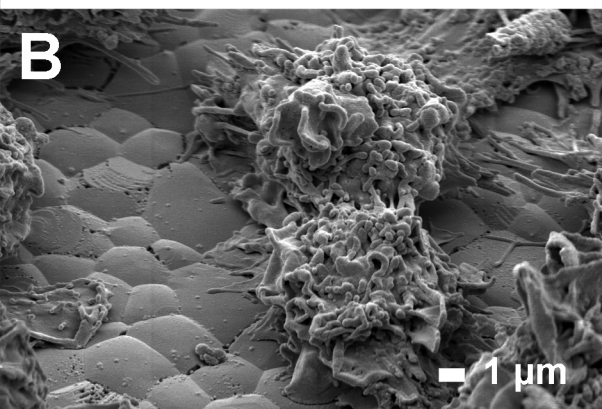
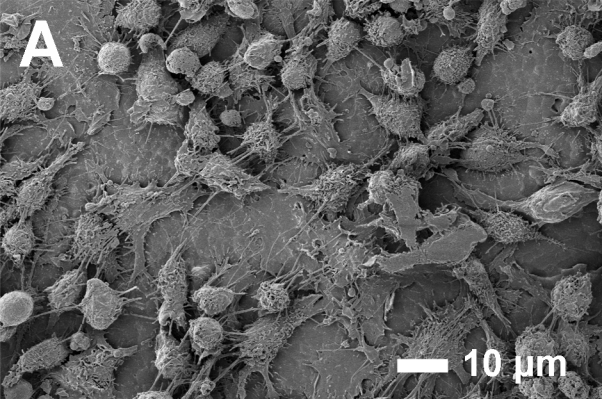
REFERENCES

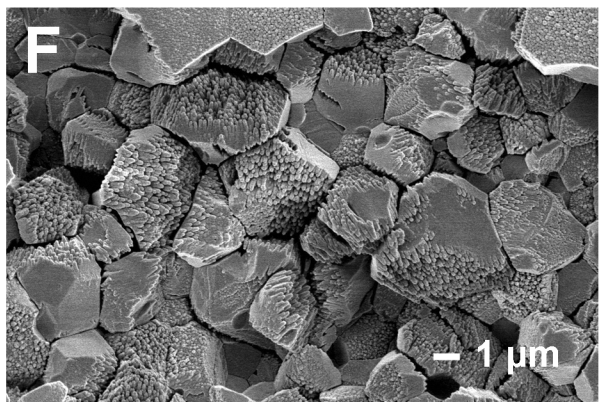
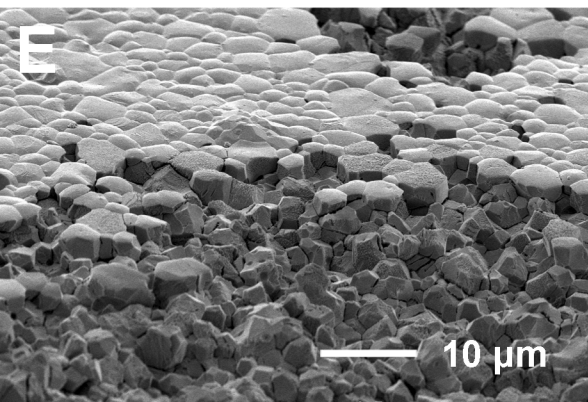
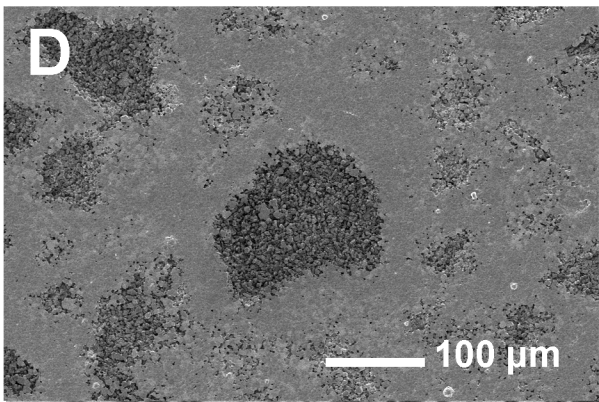
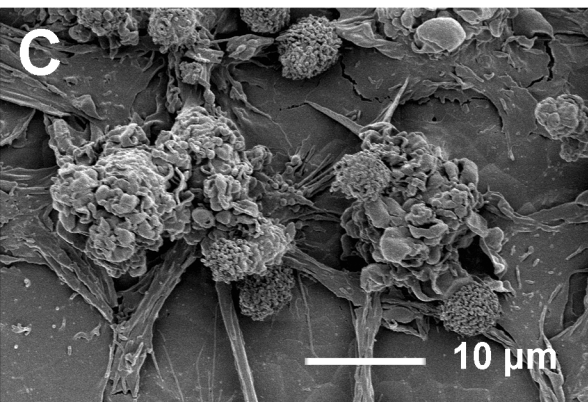
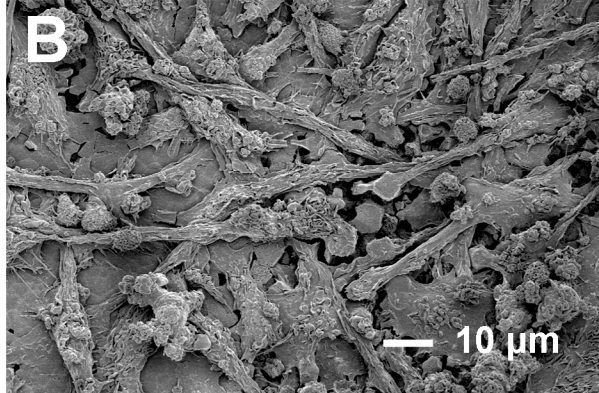
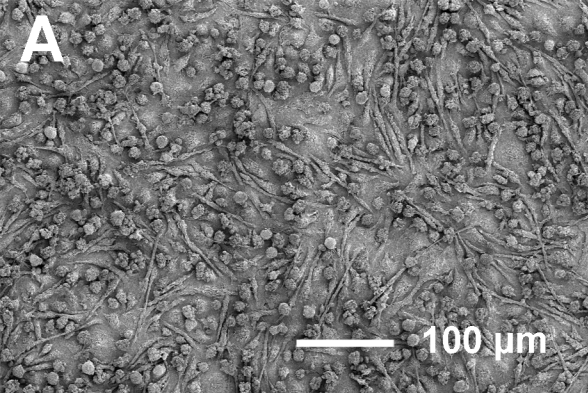
- Arbez, B. and Libouban, H., 2017. Behavior of macrophage and osteoblast cell lines in contact with the beta-TCP biomaterial (beta-tricalcium phosphate). *Morphologie* 101, 154-163.
- Asotra, S., Gupta, A., Sodek, J., Aubin, J. and Heersche, J., 1994. Carbonic anhydrase II mRNA expression in individual osteoclasts under “resorbing” and “nonresorbing” conditions. *J. Bone Miner. Res.* 9, 1115-1122.
- Barbeck, M., Booms, P., Unger, R., Hoffmann, V., Sader, R., Kirkpatrick, C.J. and Ghanaati, S., 2017. Multinucleated giant cells in the implant bed of bone substitutes are foreign body giant cells—New insights into the material-mediated healing process. *J. Biomed. Mater. Res. - Part A* 105, 1105-1111.
- Baslé, M.F., Chappard, D., Grizon, F., Filmon, R., Delecrin, J., Daculsi, G. and Rebel, A., 1993. Osteoclastic resorption of Ca-P biomaterials implanted in rabbit bone. *Calcif. Tissue Int.* 53, 348-356.
- Beuvelot, J., Pascaretti-Grizon, F., Filmon, R., Moreau, M.F., Baslé, M.F. and Chappard, D., 2011. In vitro assessment of osteoblast and macrophage mobility in presence of beta-TCP particles by videomicroscopy. *J. Biomed. Mater. Res. - Part A* 96, 108-115.
- Bohner, M., Galea, L. and Doebelin, N., 2012. Calcium phosphate bone graft substitutes: Failures and hopes. *J. Europ. Ceramic Soc.* 32, 2663-2671.
- Chamberlain, L.M., Godek, M.L., Gonzalez-Juarrero, M. and Grainger, D.W., 2009. Phenotypic non-equivalence of murine (monocyte-) macrophage cells in biomaterial and inflammatory models. *J. Biomed. Mater. Res. - Part A* 88, 858-871.
- Chappard, D., Guillaume, B., Mallet, R., Pascaretti-Grizon, F., Baslé, M.F. and Libouban, H., 2010. Sinus lift augmentation and beta-TCP: a microCT and histologic analysis on human bone biopsies. *Micron* 41, 321-326.
- Chinga, G., Johnsen, P.O., Dougherty, R., Berli, E.L. and Walter, J., 2007. Quantification of the 3D microstructure of SC surfaces. *J. Microsc.* 227, 254-265.
- Clarke, S.A., Martin, J., Nelson, J., Hornez, J.C., Bohner, M., Dunne, N. and Buchanan, F., 2017. Surrogate outcome measures of in vitro osteoclast resorption of beta tricalcium phosphate. *Adv. Healthcare Mater.* 6.
- Ćurković, L., Jelača, M.F. and Kurajica, S., 2008. Corrosion behavior of alumina ceramics in aqueous HCl and H₂SO₄ solutions. *Corrosion Sci.* 50, 872-878.
- Davison, N.L., ten Harkel, B., Schoenmaker, T., Luo, X., Yuan, H., Everts, V., Barrere-de Groot, F. and de Bruijn, J.D., 2014. Osteoclast resorption of beta-tricalcium phosphate controlled by surface architecture. *Biomaterials* 35, 7441-7451.
- Dersot, J., Colombier, M., Lafont, J., Baroukh, B., Septier, D. and Saffar, J., 1995. Multinucleated giant cells elicited around hydroxyapatite particles implanted in craniotomy defects are not osteoclasts. *Anat. Rec.* 242, 166-176.
- Detsch, R., Mayr, H. and Ziegler, G., 2008. Formation of osteoclast-like cells on HA and TCP ceramics. *Acta Biomater.* 4, 139-148.
- Detsch, R., Schaefer, S., Deisinger, U., Ziegler, G., Seitz, H. and Leukers, B., 2010. In vitro -Osteoclastic Activity Studies on Surfaces of 3D Printed Calcium Phosphate Scaffolds. *J. Biomater. Appl.* 26, 359-380.

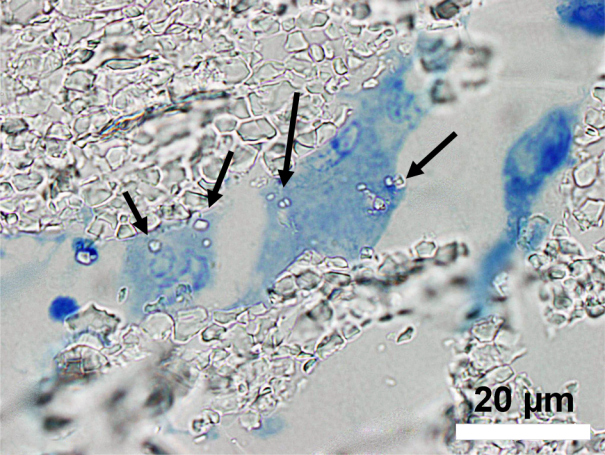
- Dorozhkin, S.V., 2017. Calcium orthophosphates (CaPO₄): Occurrence and properties. *Morphologie* 101, 125-142.
- Eggl, P.S., Müller, W. and Schenk, R.K., 1987. Porous Hydroxyapatite and Tricalcium Phosphate Cylinders with Two Different Pore Size Ranges Implanted in the Cancellous Bone of Rabbits. *Clin. Orthop. Rel. Res.* 232.
- Guillaume, B., 2017. Filling bone defects with beta-TCP in maxillofacial surgery: A review. *Morphologie* 101, 113-119.
- Halleen, J.M., Räsänen, S., Salo, J.J., Reddy, S.V., Roodman, G.D., Hentunen, T.A., Lehenkari, P.P., Kaija, H., Vihko, P. and Väänänen, H.K., 1999. Intracellular fragmentation of bone resorption products by reactive oxygen species generated by osteoclastic tartrate-resistant acid phosphatase. *J. Biol. Chem.* 274, 22907-22910.
- Hernigou, P., Dubory, A., Pariat, J., Potage, D., Roubineau, F., Jammal, S. and Flouzat Lachaniette, C.H., 2017. Beta-tricalcium phosphate for orthopedic reconstructions as an alternative to autogenous bone graft. *Morphologie* 101, 173-179.
- Jacob, S.S. and Sudhakaran, P., 2001. Monocyte–macrophage differentiation in three dimensional collagen lattice. *Bioch. Biophys. Acta.-Mol. Cell Res.* 1540, 50-58.
- Karhukorpi, E.-K., 1991. Carbonic anhydrase II in rat acid secreting cells: comparison of osteoclasts with gastric parietal cells and kidney intercalated cells. *Acta Histochem.* 90, 11-20.
- Kishi, Y., Shimojima, H., Ohsio, S., Saitoh, H. and Uematsu, K., 1997. Microstructure design of HIPed TiO₂ ceramics for improved corrosion resistance. *J. Mater. Sci. Lett.* 16, 1342-1344.
- Kucera, T., Sponer, P., Urban, K. and Kohout, A., 2014. Histological assessment of tissue from large human bone defects repaired with beta-tricalcium phosphate. *Eur J Orthop Surg Traumatol* 24, 1357-1365.
- Kumar, P.N., Mishra, S.K. and Kannan, S., 2015. Probing the limit of magnesium uptake by β -tricalcium phosphate in biphasic mixtures formed from calcium deficient apatites. *J. Solid State Chem.* 231, 13-19.
- Laitala, T. and Väänänen, K., 1993. Proton channel part of vacuolar H⁺-ATPase and carbonic anhydrase II expression is stimulated in resorbing osteoclasts. *J. Bone Miner. Res.* 8, 119-126.
- Lange, T., Schilling, A.F., Peters, F., Haag, F., Morlock, M.M., Rueger, J.M. and Amling, M., 2009. Proinflammatory and osteoclastogenic effects of beta-tricalciumphosphate and hydroxyapatite particles on human mononuclear cells in vitro. *Biomaterials* 30, 5312-5318.
- Lees, R.L., Sabharwal, V.K. and Heersche, J.N., 2001. Resorptive state and cell size influence intracellular pH regulation in rabbit osteoclasts cultured on collagen-hydroxyapatite films. *Bone* 28, 187-194.
- Lyu, S.-Y. and Park, W.-B., 2005. Production of cytokine and NO by RAW 264.7 macrophages and PBMC in vitro incubation with flavonoids. *Arch. Pharm. Res.* 28, 573.
- Mabilleau, G., Pascaretti-Grizon, F., Baslé, M.F. and Chappard, D., 2012. Depth and volume of resorption induced by osteoclasts generated in the presence of RANKL, TNF-alpha/IL-1 or LIGHT. *Cytokine* 57, 294-299.
- Mikeska, K.R., Bennison, S.J. and Grise, S.L., 2000. Corrosion of Ceramics in aqueous hydrofluoric acid. *J. Am. Ceram. Soc.* 83, 1160-1164.

- Murray, D.W. and Rushton, N., 1990. Macrophages stimulate bone resorption when they phagocytose particles. *J. Bone Joint Surg. Am.* 72-B.
- Nyangoga, H., Aguado, E., Goyenvalle, E., Baslé, M.F. and Chappard, D., 2010. A non-steroidal anti-inflammatory drug (ketoprofen) does not delay beta-TCP bone graft healing. *Acta Biomater.* 6, 3310-3317.
- Pascaretti-Grizon, F., Guillaume, B., Terranova, L., Arbez, B., Libouban, H. and Chappard, D., 2017. Maxillary sinus lift with beta-tricalcium phosphate (beta-TCP) in edentulous patients: a nanotomographic and raman study. *Calcif. Tissue Int.* 101, 280-290.
- Pascaretti-Grizon, F., Mabilieu, G., Baslé, M.F. and Chappard, D., 2011. Measurement by vertical scanning profilometry of resorption volume and lacunae depth caused by osteoclasts on dentine slices. *J. Microsc.* 241, 147-152.
- Roy, M., Fielding, G., Bandyopadhyay, A. and Bose, S., 2013. Effects of zinc and strontium substitution in tricalcium phosphate on osteoclast differentiation and resorption. *Biomater Sci* 1, 74-82.
- Schaefer, S., Detsch, R., Uhl, F., Deisinger, U. and Ziegler, G., 2011. How degradation of calcium phosphate bone substitute materials is influenced by phase composition and porosity. *Adv. Eng. Mater.* 13, 342-350.
- Suba, Z., Takacs, D., Matusovits, D., Barabas, J., Fazekas, A. and Szabo, G., 2006. Maxillary sinus floor grafting with beta-tricalcium phosphate in humans: density and microarchitecture of the newly formed bone. *Clin. Oral Implants Res.* 17, 102-108.
- Sundquist, K., Leppilampi, M., Järvelin, K., Kumpulainen, T. and Väänänen, H., 1987. Carbonic anhydrase isoenzymes in isolated rat peripheral monocytes, tissue macrophages, and osteoclasts. *Bone* 8, 33-38.
- Tai, S., Cheng, J.Y., Ishii, H., Shimono, K., Zangiacomì, V., Satoh, T., Hosono, T., Suzuki, E., Yamaguchi, K. and Maruyama, K., 2016. Effects of beta-tricalcium phosphate particles on primary cultured murine dendritic cells and macrophages. *Int. Immunopharmacol.* 40, 419-427.
- Tanaka, T., Komaki, H., Chazono, M., Kitasato, S., Kakuta, A., Akiyama, S. and Marumo, K., 2017. Basic research and clinical application of beta-tricalcium phosphate (beta-TCP). *Morphologie* 101, 164-172.
- Xia, Z., Grover, L., Huang, Y., Adamopoulos, I., Gbureck, U., Triffitt, J., Shelton, R. and Barralet, J., 2006a. In vitro biodegradation of three brushite calcium phosphate cements by a macrophage cell-line. *Biomaterials* 27, 4557-4565.
- Xia, Z., Huang, Y., Adamopoulos, I.E., Walpole, A., Triffitt, J.T. and Cui, Z., 2006b. Macrophage-mediated biodegradation of poly (DL-lactide-co-glycolide) in vitro. *J. Biomed. Mater. Res. Part A* 79, 582-590.
- Zerbo, I.R., Bronckers, A.L., de Lange, G. and Burger, E.H., 2005. Localisation of osteogenic and osteoclastic cells in porous beta-tricalcium phosphate particles used for human maxillary sinus floor elevation. *Biomaterials* 26, 1445-1451.
- Zhang, Z., Egaña, J.T., Reckhenrich, A.K., Schenck, T.L., Lohmeyer, J.A., Schantz, J.T., Machens, H.-G. and Schilling, A.F., 2012. Cell-based resorption assays for bone graft substitutes. *Acta Biomater.* 8, 13-19.
- Zuckerman, S.H., Ackerman, S. and Douglas, S., 1979. Long-term human peripheral blood monocyte cultures: establishment, metabolism and morphology of primary human monocyte-macrophage cell cultures. *Immunology* 38, 401.

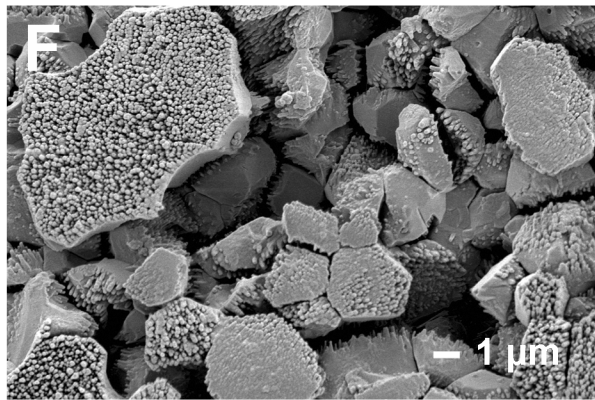
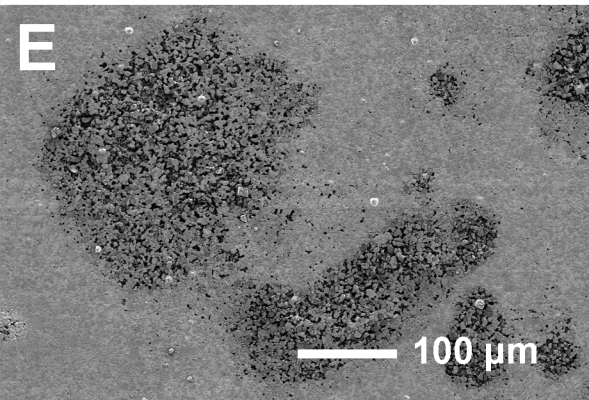
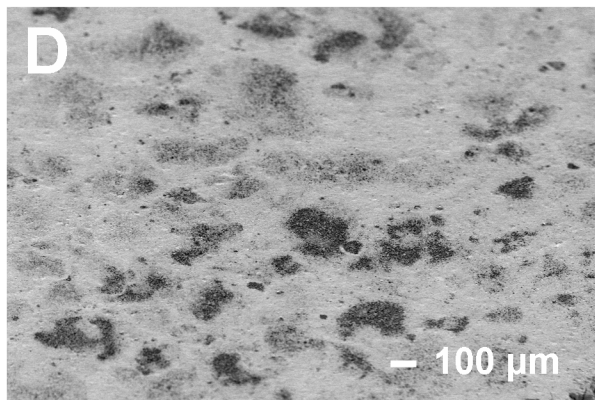
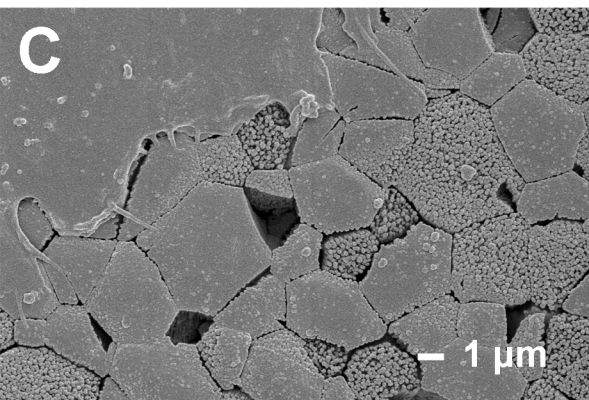
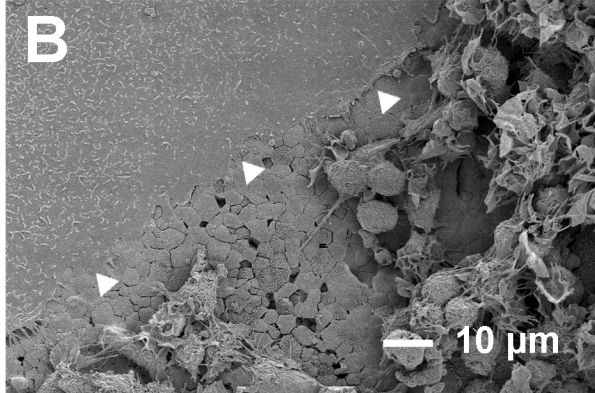
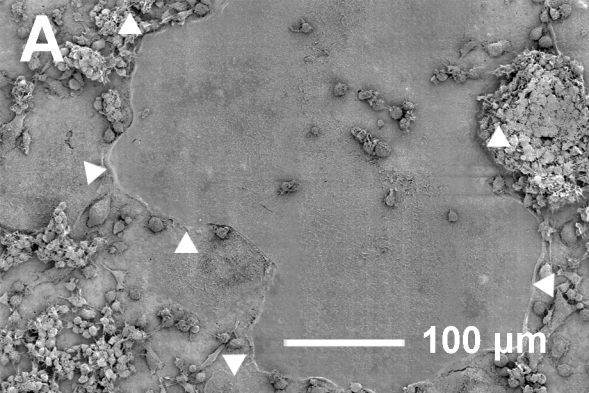


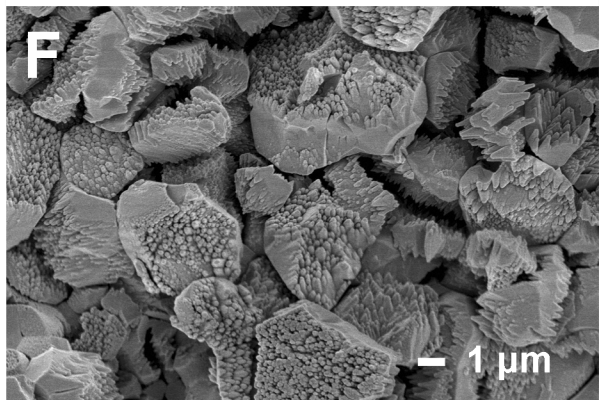
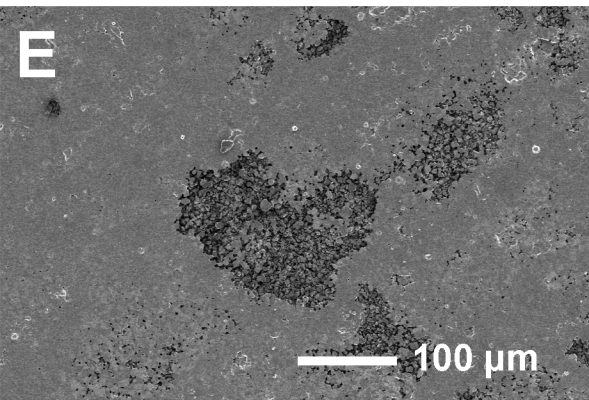
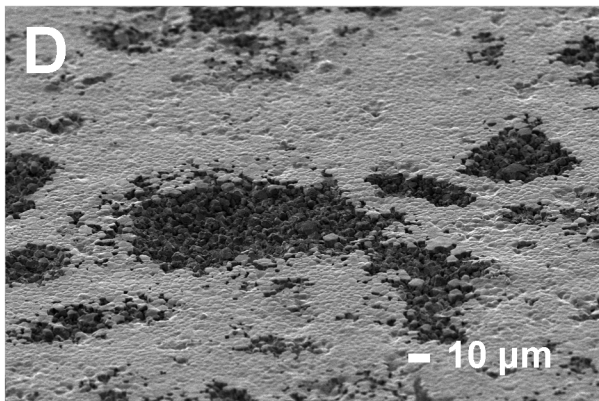
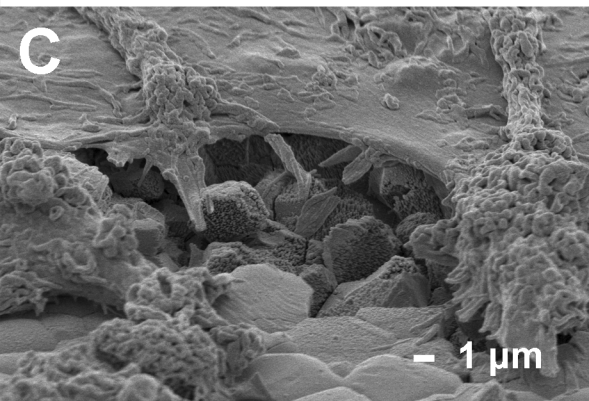
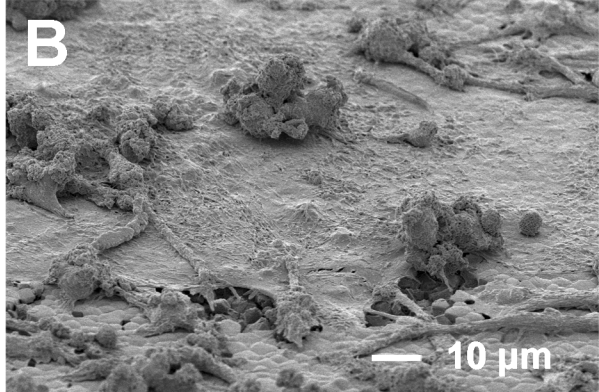
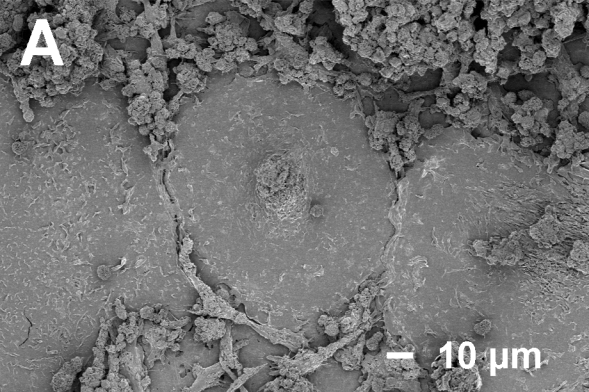


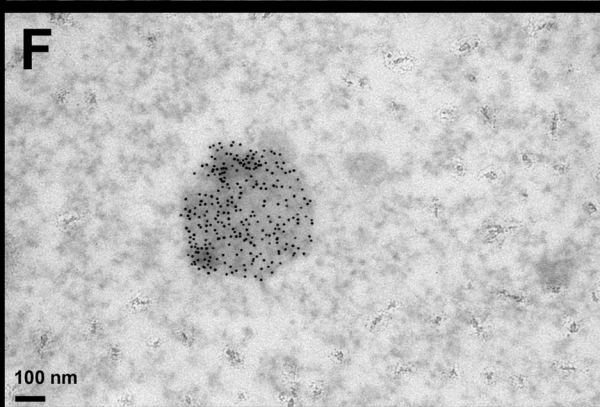
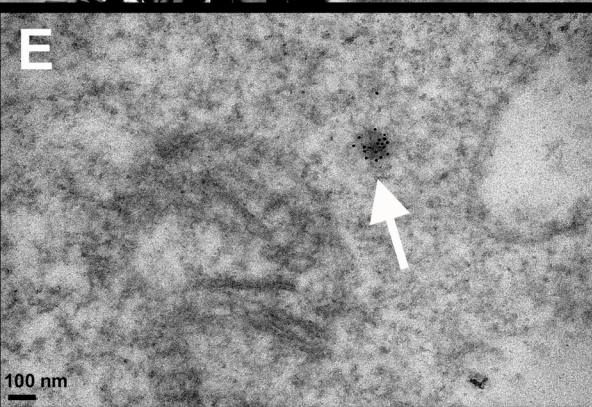
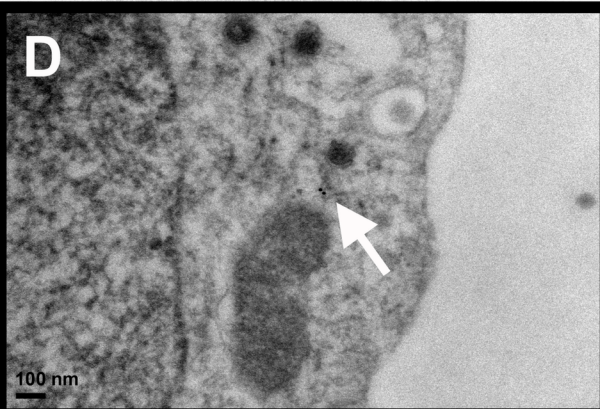
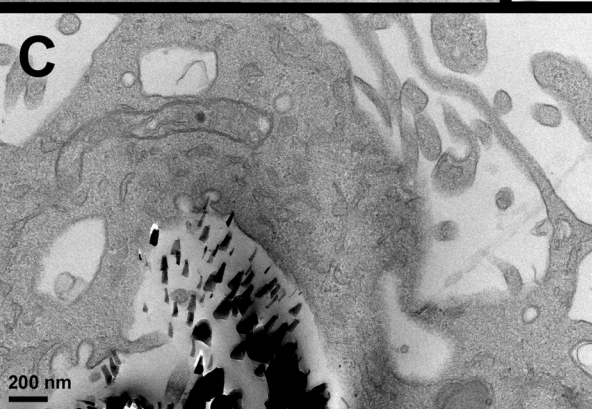
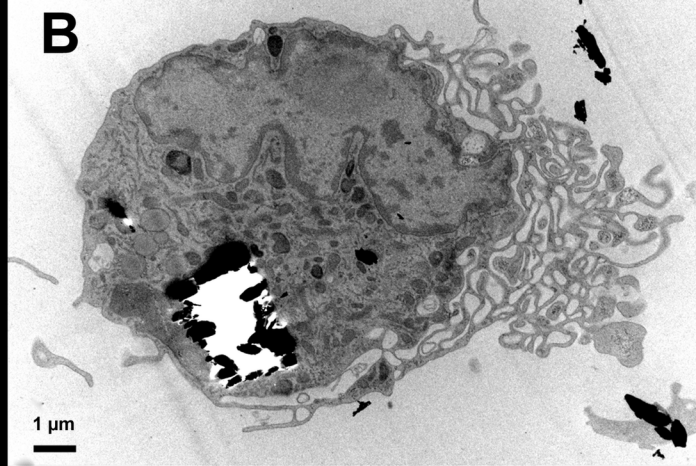
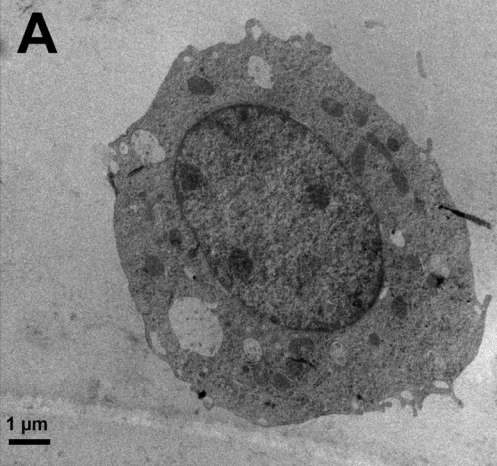




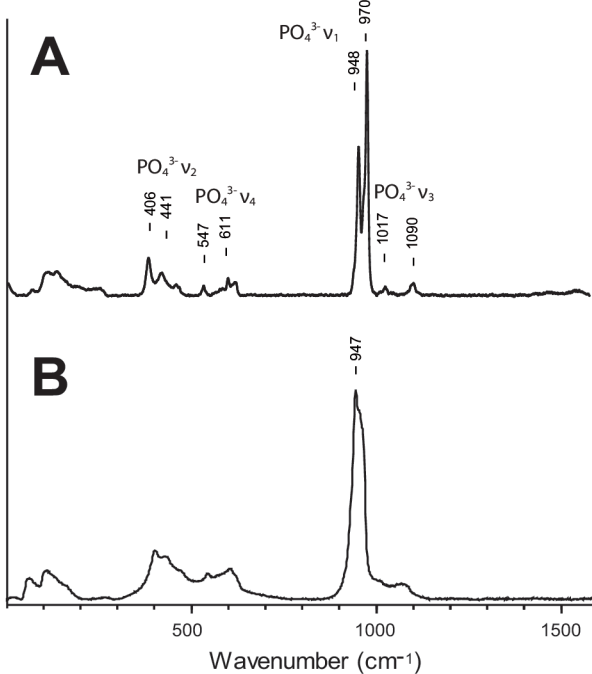
20 μm

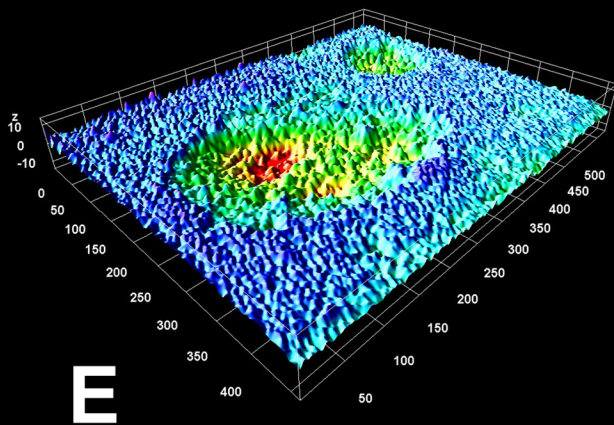
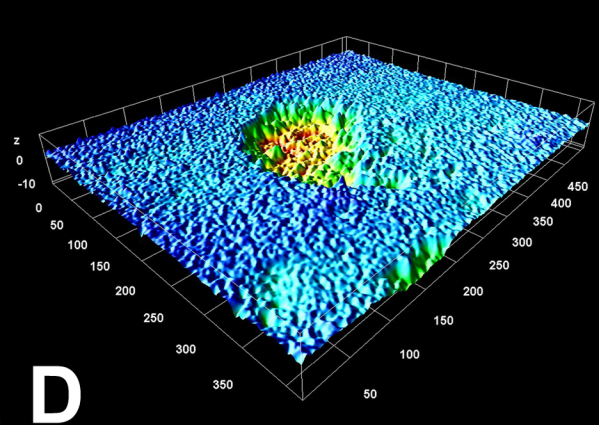
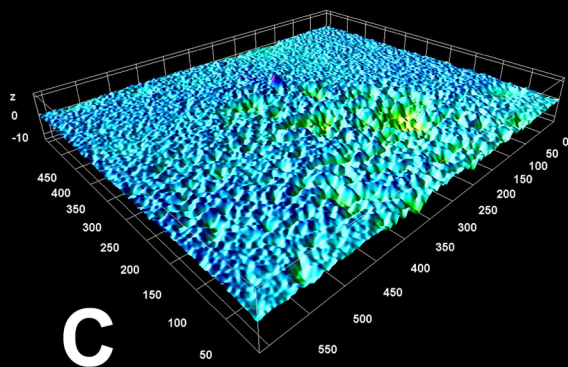
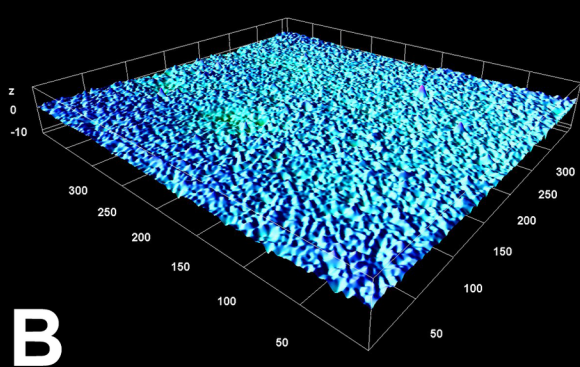
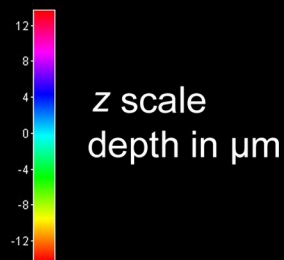
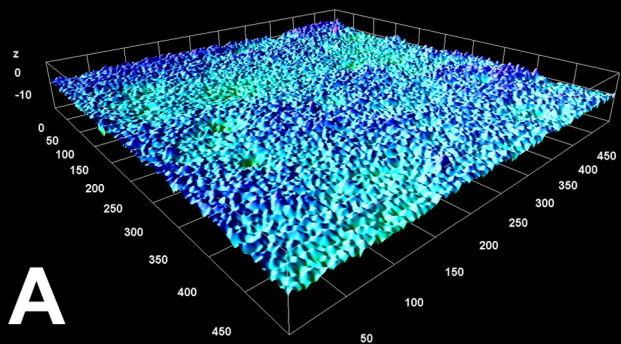


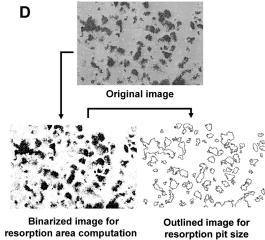
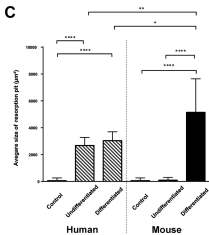
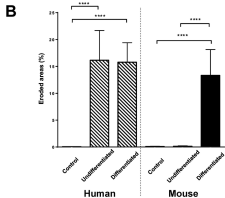
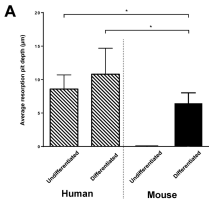




Raman intensity (arbitrary units)







Macrophages and osteoclasts on β -TCP

